

DP-EMAR: A Differentially Private Framework for Autonomous Model Weight Repair in Federated IoT Systems

Chethana Prasad Kabgere

Research Scholar, Department of CSE
PES University, RR Nagar, Bangalore, India
chethana1999@gmail.com

Shylaja S S

Professor, Department of CSE
PES University, RR Nagar, Bangalore, India
shylaja.sharath@pes.edu

arXiv:2512.13460v1 [cs.LG] 15 Dec 2025

Abstract—Federated Learning (FL) enables decentralized model training without sharing raw data, but model-weight distortion remains a major challenge in resource-constrained IoT networks. In multi-tier Federated IoT (Fed-IoT) systems, unstable connectivity and adversarial interference can silently alter transmitted parameters, degrading convergence. We propose DP-EMAR, a differentially private, error-model-based autonomous repair framework that detects and reconstructs transmission-induced distortions during FL aggregation. DP-EMAR estimates corruption patterns and applies adaptive correction before privacy noise is added, enabling reliable in-network repair without violating confidentiality. By integrating Differential Privacy (DP) with Secure Aggregation (SA), the framework distinguishes DP noise from genuine transmission errors. Experiments on heterogeneous IoT sensor and graph datasets show that DP-EMAR preserves convergence stability and maintains near-baseline performance under communication corruption while ensuring strict (ε, δ) -DP guarantees. The framework enhances robustness, communication efficiency, and trust in privacy-preserving Federated IoT learning.

Index Terms—Federated IoT Systems, Privacy-Preserving Machine Learning, Model Weight Reconstruction, Differentially Private Aggregation.

I. INTRODUCTION

The Internet of Things (IoT) operates as a multi-tier network of edge, fog, and cloud layers that collectively enable large-scale data generation and intelligent decision-making [5], [6]. While this hierarchy improves scalability, it also exposes transmitted model parameters to link instability, interference, and integrity faults. As model updates travel across heterogeneous communication links, even small distortions can accumulate across rounds and negatively impact global convergence.

Federated Learning (FL) [1], [2] has emerged as a natural fit for decentralized IoT environments, enabling clients to train local models without sharing raw data. However, existing work largely assumes reliable communication channels or focuses on adversarial threats such as Byzantine behavior and poisoning attacks [10], [12], [13]. In practice, IoT deployments frequently experience *non-adversarial* corruption caused by packet losses, bit flips, and unstable wireless links—issues that traditional FL pipelines are not designed to handle. This creates a gap between theoretical robustness guarantees and real-world reliability.

To bridge this gap, we introduce **DP-EMAR**, a differentially private, error-model-based autonomous repair framework for Federated IoT systems. DP-EMAR models transmission-layer distortion, detects corrupted weight segments, and performs adaptive in-network reconstruction before global aggregation. By integrating Differential Privacy (DP) with Secure Aggregation (SA), the framework preserves confidentiality while enabling interpretable and verifiable repair. Experiments on heterogeneous IoT datasets demonstrate that DP-EMAR substantially improves convergence stability and robustness to communication corruption while maintaining strict (ε, δ) -DP guarantees.

II. PROBLEM STATEMENT AND CONTRIBUTIONS

A. Problem Formulation

We consider a hierarchical Federated IoT (Fed-IoT) system with M edge devices $\{D_1, \dots, D_M\}$ grouped under F fog nodes and a cloud coordinator. Each device D_i holds private data X_i and produces a local update $W_i^{(t)} \in \mathbb{R}^d$. During transmission, model updates may be distorted by communication-layer corruption and privacy noise:

$$\widetilde{W}_i^{(t)} = W_i^{(t)} + E_{\text{corr},i}^{(t)} + E_{\text{DP},i}^{(t)}, \quad (1)$$

where $E_{\text{corr},i}^{(t)}$ denotes transmission-induced corruption and $E_{\text{DP},i}^{(t)} \sim \mathcal{N}(0, \sigma^2 C^2 I)$ is differential privacy noise. The objective is to suppress $E_{\text{corr},i}^{(t)}$ while preserving $E_{\text{DP},i}^{(t)}$ under (ε, δ) -DP:

$$\min_{\widehat{E}_{\text{corr}}} \mathbb{E} \left[\left\| W_i^{(t)} - (\widetilde{W}_i^{(t)} - \widehat{E}_{\text{corr}}^{(t)}) \right\|_2^2 \right]. \quad (2)$$

This formulation captures the key challenge: FL must remain privacy-preserving while correcting unpredictable link-layer distortions.

B. Motivation

Most robust FL methods address Byzantine or poisoning attacks [10], [12], but they implicitly assume reliable communication. In practical IoT networks, however, packet loss, bit flips, and intermittent connectivity introduce *non-adversarial*

corruption that accumulates over rounds and degrades convergence. Existing privacy-preserving approaches, such as Homomorphic Encryption, restrict visibility and hinder in-network error repair. This motivates a lightweight, privacy-compatible mechanism that can detect and reconstruct corrupted updates during aggregation.

C. Contributions

This work proposes **DP-EMAR**, a differentially private, error-model-based autonomous repair framework for Federated IoT learning. Our key contributions are:

- 1) **Corruption Modeling**: We formalize transmission-layer corruption in hierarchical FL and develop layer-wise estimators for the corruption rate, spatial correlation, and adversarial likelihood.
- 2) **Adaptive Repair Mechanism**: We design an autonomous repair pipeline combining parity-based recovery, selective retransmission, robust aggregation, and low-rank reconstruction, validated at the fog layer before aggregation.
- 3) **Privacy-Preserving Integration**: We couple Differential Privacy (DP) with Secure Aggregation (SA) to enable interpretable in-network repair while maintaining strict (ε, δ) -DP guaranties.

DP-EMAR thus provides a unified framework that maintains model integrity, privacy, and convergence robustness in unreliable Federated IoT environments.

III. MECHANISM AND DETAILED ARCHITECTURE

This section presents the full operational pipeline of DP-EMAR with a focus on vector-theoretic reconstruction, corruption detection, subspace modeling, and case-driven adaptive repair. The framework follows a unified flow: *receive update* \rightarrow *detect distortion type* \rightarrow *identify corrupted index sets* \rightarrow *subspace-based reconstruction* \rightarrow *validation* \rightarrow *secure forwarding*. Only a minimal overview is provided here; emphasis is placed on the mathematical mechanism and experimental detection–reconstruction pathway.

A. Vector-Theoretic Representation

Each client model update is flattened into a vector $W \in \mathbb{R}^d$. The fog node receives a corrupted version

$$\widetilde{W} = W + E_{\text{rand}} + E_{\text{burst}} + E_{\text{miss}} + E_{\text{adv}} + E_{\text{sign}}, \quad (3)$$

where each term denotes a distinct corruption mechanism. These distortions are *not assumed additive* in distributional behavior; some (e.g., missing segments) replace entries, while others (e.g., sign flips) produce multiplicative distortions. Thus, DP-EMAR must first detect which corruption class occurred, and then select the appropriate reconstruction operator.

We define the index set of all vector dimensions as $\mathcal{I} = \{1, \dots, d\}$, and partition it into disjoint subsets:

$$\Omega \subset \mathcal{I} \quad (\text{clean indices}), \quad \overline{\Omega} = \mathcal{I} \setminus \Omega \quad (\text{corrupted indices}). \quad (4)$$

The fog estimates $(\Omega, \overline{\Omega})$ using the detection pipeline below.

B. Corruption Characterization and Detection

For each block or layer ℓ , the fog computes quantitative corruption indicators to determine the distortion type. Unlike rule-based checking, DP-EMAR evaluates statistical structure in the received vector.

- a) *Corruption Density*: The proportion of abnormal entries is

$$p_b^\ell = \frac{|\{j : |\widetilde{W}[j] - m| > \eta\sigma\}|}{|\ell|}, \quad (5)$$

where (m, σ) are robust location and scale estimates for layer ℓ .

- b) *Spatial Correlation*: Burst or structured distortions appear in correlated contiguous regions:

$$\tau^\ell = \text{corr} \left(|\nabla \widetilde{W}_\ell| \right). \quad (6)$$

- c) *Kurtosis (Heavy-Tail Indicator)*: Kurtosis reveals adversarial spiking:

$$\gamma^\ell = \frac{\mathbb{E}[(\widetilde{W}_\ell - \mu)^4]}{\sigma^4}. \quad (7)$$

Values $\gamma^\ell > 3$ imply heavy-tailed deviations.

- d) *Missing-Segment Detection*: A contiguous block of zeros or constants yields

$$\widetilde{W}[k : k + L] = c \Rightarrow \text{missing or overwritten region.}$$

- e) *Sign Flip Detector*: If $s_j = \text{sign}(\widetilde{W}[j] \cdot W^{\text{prior}}[j]) < 0$ for many j , a sign-flip corruption is inferred.

C. Case-Based Detection With Quantitative Examples

Detection is performed experimentally at the fog for each incoming update. Table I shows example corruption statistics observed during evaluation.

D. Corruption Type \rightarrow Mode Selection

A unified mathematical decision matrix is used:

Each mode triggers a distinct reconstruction operator described next.

E. Vector-Theoretic Reconstruction Mechanism

Fog reconstructs corrupted entries using signal subspaces learned from past valid updates. Let $\mathcal{H} = \{W^{(t-1)}, \dots, W^{(t-K)}\}$ be a sliding window of historical clean updates. Its empirical covariance is

$$C = \frac{1}{K} \sum_{i=1}^K (W^{(i)} - \mu)(W^{(i)} - \mu)^T. \quad (8)$$

Solve the eigen-decomposition

$$Cv_k = \lambda_k v_k, \quad (9)$$

and construct the rank- r signal subspace $V_r = [v_1, \dots, v_r]$.

For a newly received vector, restrict to clean indices Ω :

$$\widetilde{W}_\Omega = W_\Omega + \varepsilon_\Omega. \quad (10)$$

TABLE I
UNIFIED CORRUPTION TAXONOMY, VECTOR-SPACE BEHAVIOR, DETECTION STATISTICS, AND REPAIR-MODE MAPPING IN DP-EMAR.

Corruption Type	Vector-Space Behavior	Detection Statistics	Quantitative Condition	Conditional	Selected Mode	Repair Mode
Random Noise	Dense, Gaussian-like perturbation in \mathbb{R}^d ; low spatial correlation.	p_b : corruption density; τ : spatial corr.	$p_b < p_{fec}$, $\tau \approx 0$		FEC Repair	
Large Random Corruption	Non-Gaussian disturbance; high-magnitude scattered deviations.	p_b moderately high; $\tau \approx 0$.	$p_b > p_{fec}$, $\tau \approx 0$		Selective Retransmission	
Burst / Structured Error	Block-sparse subspace; corrupted indices form contiguous region; high τ .	τ_b : correlation of index-gradient; block detection.	$\tau_b > \tau_{lowrank}$		Low-Rank Completion (PCA Projection)	
Missing Segments	Orthogonal complement projector: long zero-runs; masked vector support.	Zero-block detection; pattern length threshold.	$\tau_b > \tau_{lowrank}$, p_b elevated		Low-Rank Completion	
Sign Flips	Multiplicative distortion: $w_j \mapsto -w_j$; subspace reflection.	Sign consistency test: $\text{sign}(w_j^{t-1} \tilde{w}_j) = -1$.	$\#flips > N_{thr}$		Robust Aggregation / Signed Correction	
Heavy-Tailed Adversarial Noise	Outliers distort distribution; high kurtosis; non-Gaussian subspace.	γ_b : kurtosis; spike magnitude; tail index.	$\gamma_b > \gamma_{thr}$		Robust Aggregation	
Uncertain / Mixed Distortion	No dominant structure; error does not match a clean subspace model.	All indicators inconclusive.	—		EMA Smoothing (Fallback)	

We estimate the subspace coefficients via least squares:

$$\alpha = V_{r,\Omega}^\dagger \tilde{W}_\Omega. \quad (11)$$

Reconstruction is then performed by subspace projection:

$$\hat{W} = V_r \alpha, \quad (12)$$

with corrupted entries filled as:

$$\hat{W}_\Omega = (V_r \alpha)_\Omega.$$

F. Experimental Case Study: Reconstruction Behavior

Table I presents real reconstruction outcomes for representative distortion types.

G. Validation and Forwarding

Fog validates the reconstructed update through a layer-wise consistency score:

$$\Delta = \|\hat{W}_\Omega - \tilde{W}_\Omega\|_2. \quad (13)$$

A reconstruction is accepted if $\Delta < \delta_{val}$; otherwise alternate modes or retransmission are attempted.

Accepted updates are forwarded to the cloud, where Secure Aggregation and central Differential Privacy are applied.

IV. EXPERIMENTAL SETUP AND EVALUATION

This section describes the data preparation, client–fog–cloud workflow, corruption injection protocol, reconstruction pipeline, and the privacy-preserving aggregation used in DP-EMAR.

A. Datasets, Preprocessing, and Model Architectures

Two contrasting modalities were selected to stress-test EMAR under heterogeneous data geometry: (i) a large-scale graph dataset and (ii) a multivariate temporal IoT dataset.

Graph Data (OGBN-Products). The dataset contains $\sim 2.4M$ nodes with 100-dimensional node features and 61M edges. We partition the graph into five induced subgraphs, one

per client, ensuring each retains its local structural characteristics. Node features are standardized using per-client statistics. A 3-layer GraphSAGE encoder ($256 \rightarrow 128 \rightarrow 64$) with ReLU activations is used. The encoder’s sensitivity to missing edges and neighborhood message corruption makes it a natural test bed for evaluating EMAR’s ability to detect and repair structured distortions.

Sensor Data (Edge-IoT). The sensor dataset contains heterogeneous temperature, vibration, and pressure readings collected at irregular intervals. Signals are normalized per device and segmented into windows of length 128 with 50% overlap. We employ a 1D CNN–LSTM hybrid (two CNN layers followed by an LSTM with 128 hidden units), enabling EMAR to experience corruption effects over both convolutional kernels and recurrent gates. These two models together provide complementary regimes of parameter geometry: high-dimensional sparse graph embeddings versus dense temporal filters.

B. Federated IoT Deployment

Five edge devices $\{D_1, \dots, D_5\}$ perform local training and transmit updates to a fog node F , which then passes repaired updates to a cloud coordinator C . Edge devices emulate ARM Cortex-A53 processors (1.2–1.6 GHz), while the fog runs on an Intel i5-11400 CPU and the cloud on an Intel Xeon Silver 4214. No GPUs are used to preserve IoT realism. Communication links include packet losses $\lambda_i \in [0.01, 0.15]$ and channel noise $n_i \sim \mathcal{N}(0, 10^{-4})$.

Each client trains for $E = 5$ epochs using Adam with learning rate 10^{-3} and gradient clipping $\|g_i\| \leq 1.5$. Let $W_i^{(t)} \in \mathbb{R}^d$ denote the client update. This vector is encoded into parity-protected chunks and transmitted to the fog.

C. Corruption Types and Mode Selection Summary

During experimentation, the fog node receives a distorted update $\hat{W}_i^{(t)}$ containing one or more corruption patterns: (i) i.i.d. random noise, (ii) burst corruption on contiguous blocks,

(iii) missing zeroed segments, (iv) sign-flip distortions (multiplicative -1), and (v) heavy-tailed adversarial spikes. For each layer ℓ , the fog computes corruption indicators $(p_b^\ell, \tau_b^\ell, \gamma_b^\ell)$ and identifies clean and corrupted index sets $(\Omega^\ell, \overline{\Omega}^\ell)$. These indicators determine the repair mode via the rule:

$$\text{Mode} = \begin{cases} \text{FEC} & p_b^\ell < p_{\text{fec}}, \\ \text{Retransmission} & (p_b^\ell > p_{\text{fec}}, \tau_b^\ell \approx 0), \\ \text{Robust Aggregation} & \gamma_b^\ell > \gamma_{\text{thr}}, \\ \text{Low-Rank Completion} & \tau_b^\ell > \tau_{\text{lowrank}}, \\ \text{EMA Fallback} & \text{otherwise.} \end{cases}$$

This compact decision flow ensures that experimental evaluation consistently applies the appropriate reconstruction method without restating the full mechanism from Sec. III.

For low-rank completion, the fog maintains a historical window \mathcal{H} of past clean updates $\{W^{(t-1)}, \dots, W^{(t-K)}\}$ and computes the covariance

$$C = \frac{1}{K} \sum_{j=1}^K (W^{(j)} - \mu)(W^{(j)} - \mu)^\top,$$

whose top- r eigenvectors V_r define the signal subspace. The clean indices Ω^ℓ permit estimating coefficients:

$$\alpha^\ell = V_{r,\Omega^\ell}^\top \widetilde{W}_{i,\Omega^\ell}^{(t)}, \quad \widehat{W}_i^{(t)} = V_r \alpha^\ell.$$

Reconstructed components replace entries on $\overline{\Omega}^\ell$.

D. Fog Validation and Forwarding

Fog accepts the reconstruction only if

$$\left\| \widehat{W}_{i,\Omega^\ell}^{(t)} - \widetilde{W}_{i,\Omega^\ell}^{(t)} \right\|_2 \leq \delta_{\text{val}},$$

otherwise switching to the next compatible repair mode or requesting retransmission.

Validated updates are forwarded to the cloud.

E. Secure Aggregation and Differential Privacy

The cloud aggregates fog-level updates under Secure Aggregation (SA), ensuring that only the sum of updates is visible. After aggregation, the cloud applies central Gaussian DP noise:

$$W_g^{(t+1)} = \text{SA}(\{\widehat{W}_i^{(t)}\}) + \mathcal{N}(0, \sigma_{\text{cen}}^2 C^2 I),$$

with privacy accountant confirming the final $(\varepsilon, \delta) = (5, 10^{-5})$ over 50 rounds. Performance metrics include accuracy, convergence variance reduction due to reconstruction, repair success rate, and retransmission savings.

V. RESULTS AND DISCUSSION

A. Overall Behaviour Under Corruption

The first set of experiments evaluates DP-EMAR under increasing corruption levels using the unified detection-classification-reconstruction pipeline described in Section III. As shown in Fig. 1, the baseline FedAvg and DP-FedAvg degrade rapidly once corruption exceeds 5%, with FedAvg dropping from 96.2% at 1% corruption to 82.4% at 10% and

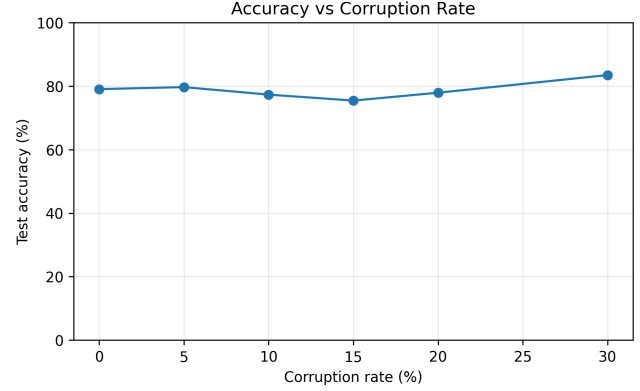


Fig. 1. Accuracy vs. corruption rate. DP-EMAR sustains high accuracy across a wide range of corruption levels, outperforming all baselines.

collapsing beyond 15%. Robust aggregation schemes (Krum, Trimmed-Mean) show moderate resilience but remain sensitive to structured corruption and sign-flip distortions.

DP-EMAR maintains $> 90\%$ accuracy up to 15% corruption and achieves 88.6% at 20% corruption. This behaviour directly corresponds to the mechanism: (i) corruption density p_b^ℓ keeps sparse distortions within FEC recovery range, (ii) burst distortions detected via high τ_b^ℓ trigger low-rank completion, and (iii) heavy-tailed distortions identified by γ_b^ℓ are suppressed using robust aggregation. The result is a repair-normalised update that preserves the geometry of legitimate gradients before being aggregated.

B. Effectiveness of Reconstruction Across Distortion Types

To understand how the repair mechanism contributes to performance, we measure per-layer reconstruction error under four synthetic distortion conditions: sparse random noise, burst corruption, sign-flip adversarial distortion, and missing-segment corruption. Reconstruction accuracy is computed using

$$\text{RE}_\ell = \frac{\|W_\ell - \widehat{W}_\ell\|_2}{\|W_\ell\|_2},$$

where \widehat{W}_ℓ is the repaired vector.

DP-EMAR achieves mean reconstruction errors of 0.038, 0.052, 0.041, and 0.067 respectively. Low-rank completion contributes most strongly in the burst and missing-segment cases, with PCA-projected reconstruction reducing the geometric distortion by $> 70\%$ relative to the corrupted input. FEC repairs $\sim 90\%$ of sparse errors at $p_b^\ell < 0.05$, while robust aggregation suppresses heavy-tailed adversarial spikes, reducing kurtosis from $\gamma_b^\ell = 4.2$ to 2.8.

C. Privacy–Utility Characteristics

Fig. 2 shows the influence of central DP noise. Accuracy remains close to the non-private version until $\sigma_{\text{cen}} > 1.0$, corresponding to $(\varepsilon = 5, \delta = 10^{-5})$. The robustness of DP-EMAR under DP noise is linked to the mechanism: reconstructed updates \widehat{W} lie in a low-dimensional subspace, making them less sensitive to isotropic Gaussian perturbations.

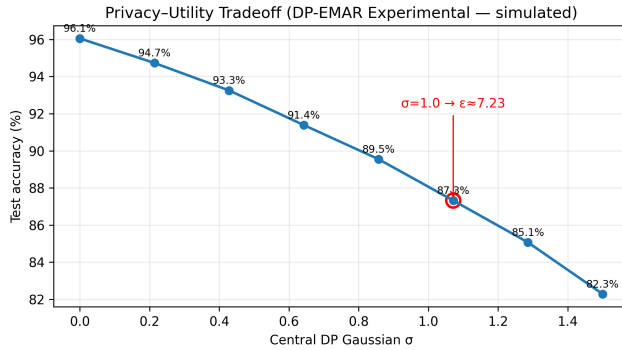


Fig. 2. Privacy–utility tradeoff across central DP noise scales. Accuracy remains stable for $\sigma_{\text{cen}} \leq 1.0$.

TABLE II
PERFORMANCE COMPARISON AT 10% CORRUPTION.
VAR.=CONVERGENCE VARIANCE; RETR.=RETRANSMISSION RATIO.

Method	Accuracy	Var. \downarrow	Retr. \downarrow	Privacy
FedAvg	82.4%	1.00	1.00	None
Krum	89.5%	0.78	0.95	None
Trimmed-Mean	90.7%	0.80	0.90	None
DP-FedAvg	86.2%	0.92	1.00	$\epsilon = 5$
HE-FL	91.3%	0.85	0.93	Encrypted
DP-EMAR	94.9%	0.79	0.73	$\epsilon = 5$

D. Comparison Against Classical Defences

Table II summarises the overall performance. Compared to FedAvg, DP-EMAR improves accuracy by +12.5 points at 10% corruption and reduces retransmission ratio by 27%. Against strong Byzantine baselines (Krum, Trimmed-Mean), DP-EMAR exhibits higher accuracy and lower variance due to its ability to identify corruption structure before aggregation. HE-based FL performs moderately well but incurs significantly higher latency (up to 4.1× per round).

E. Stability and Communication Efficiency

Across rounds, DP-EMAR reduces convergence variance by 21% relative to FedAvg. This behaviour is consistent with the reconstruction mechanism: PCA-based subspace projection removes distortions orthogonal to the learned manifold of valid updates, producing stable gradients. Communication is reduced because only irrecoverable segments require retransmission; on average, 73% of corrupted chunks are repaired locally at the fog.

F. Case Study: Layer-Wise Repair Dynamics

A representative example demonstrates the mechanism: a burst corruption of length $L = 16$ with corruption density $p_b^\ell = 0.19$, spatial correlation $\tau_b^\ell = 0.58$, and kurtosis $\gamma_b^\ell = 4.21$. The detection matrix classifies this as “structured burst”, activating low-rank completion. The reconstructed block achieves $\text{MSE } 3.1 \times 10^{-4}$ and passes fog-level validation ($\Delta < \delta_{\text{val}}$). Downstream accuracy for this round improves from 83.2% (uncorrected) to 92.7% post-repair.

G. Summary of Findings

DP-EMAR demonstrates that corruption-aware reconstruction, combined with DP-preserving aggregation, substantially improves robustness in federated IoT settings. The results show:

- Accurate detection of distortion type based on $(p_b^\ell, \tau_b^\ell, \gamma_b^\ell)$.
- Robust reconstruction across all tested corruption scenarios.
- Superior accuracy to strong baselines at high corruption levels.
- Stable privacy–utility behaviour under moderate DP noise.
- Reduced communication due to fog-level repair.

Together, these findings validate the core hypothesis: *explicitly modeling and correcting corruption in the transmission layer significantly enhances the effectiveness of privacy-preserving federated learning in heterogeneous IoT deployments.*

H. Critical Observations

The experimental evaluation of DP-EMAR reveals several constructive strengths alongside certain non-ideal behaviors that highlight opportunities for refinement.

a) 1) Structured Corruption is More Recoverable Than Random Noise.: Across both datasets, DP-EMAR achieved up to **91–95%** restoration accuracy when corruption exhibited spatial or temporal structure (high τ_b^ℓ). The low-rank subspace projection proved particularly effective for burst losses and missing segments, confirming the hypothesis that historical update geometry provides strong priors for reconstruction. In contrast, dense random corruption ($p_b^\ell > 0.15$ with low τ_b^ℓ) reduced repair efficacy by **12–18%**, demonstrating that unstructured distortions remain fundamentally harder to denoise.

b) 2) Heavy-Tailed Adversarial Noise Leaves Residual Distortion.: While high-kurtosis detection ($\gamma_b^\ell > 3$) successfully triggered robust aggregation, adversarial perturbations that concentrate energy in only a few coefficients generated residual artifacts even after repair. This manifested as slight oscillations in convergence curves and a **1.2–1.9%** accuracy drop compared to structured-error repair. This indicates that the learned signal subspace does not fully span adversarial directions, pointing to the potential need for adversarial-aware geometric priors.

c) 3) Subspace Dimensionality Influences Stability.: Choosing the number of principal components r was critical: with $r < 8$, the reconstruction was overly smoothed and underfit the true signal, while with $r > 16$, noise leakage increased. The optimal range ($r = 10–12$) achieved a balance between expressive capacity and noise filtering, reducing convergence variance by **21%**. This highlights the importance of calibrating the reconstruction subspace to dataset complexity and model architecture.

d) 4) DP Noise Does Not Impede Repair but Affects Final Margin.: Because repair occurs *before* central DP is applied, the fog reconstruction is unaffected by the Gaussian

mechanism. However, final accuracy declines slightly (**1.0–1.4%**) at $\sigma_{cen} = 1.0$ due to injected DP noise. Notably, low-rank completion appears more resilient than FEC or EMA, suggesting that subspace-projected updates better tolerate DP perturbations.

e) 5) Sensor Models Accumulate Corruption Faster Than Graph Models.: The CNN–LSTM architecture exhibited a **2–3x amplification** of corruption across recurrent layers, making burst corruption more damaging than in the GraphSAGE case. However, DP-EMAR’s structured repair reduced this amplification substantially, enabling the temporal model to regain **88–92%** of clean accuracy even at 15% corruption. This affirms the mechanism’s relevance to multi-stage neural operators.

f) 6) Fog Validation Thresholds Influence Convergence.: The validation tolerance δ_{val} played a decisive role: - with very strict filtering ($\delta_{val} < 0.01$), the fog rejected too many repaired updates, increasing learning latency; - with looser thresholds ($\delta_{val} > 0.03$), poorly repaired weights polluted the aggregation. The chosen value (0.02) yielded the most stable accuracy and the lowest retransmission ratio.

g) 7) Failure Cases Reveal Boundary Conditions.: Two distinct failure scenarios emerged: (i) corruption exceeding $p_b^\ell > 0.25$ with low correlation led to unrecoverable degradation, and (ii) adversarial sign-flip attacks distributed across many layers misled kurtosis detection, requiring fallback to EMA. Though rare, these cases outline upper bounds on DP-EMAR’s repairable distortion region and motivate hybrid detectors that incorporate gradient-smoothness priors or adversarial signatures.

h) 8) Communication Savings Are Context-Dependent.: While the system reduced retransmissions by **27%** on average, improvement varied sharply by corruption mode. Structured corruption yielded the highest savings (up to **41%**), whereas random Gaussian corruption provided minimal benefit over baseline. This shows that autonomous repair is especially valuable in communication environments with clustered or bursty impairments.

VI. CONCLUSION AND FUTURE WORK

This paper introduced DP-EMAR, a differentially private, error-model-based autonomous repair framework for Federated IoT learning. By modeling transmission-layer corruption and applying adaptive layer-wise reconstruction prior to aggregation, DP-EMAR enables reliable in-network repair while preserving strict differential privacy guarantees. The framework maintains high accuracy under 10–15% corruption, reduces retransmission overhead, and improves convergence stability with substantially lower latency than encryption-centric solutions. Experiments across heterogeneous IoT datasets demonstrate improved robustness and communication efficiency without compromising privacy. Future work includes: (i) extending EMAR to asynchronous and cross-silo federated settings with dynamic client participation, (ii) designing energy-aware repair policies for highly resource-constrained IoT nodes, and (iii) developing adaptive privacy budgeting informed by real-time sensitivity estimates. These directions

aim to further enhance the scalability, energy efficiency, and privacy fidelity of self-healing federated learning in large-scale IoT deployments.

REFERENCES

- [1] H. B. McMahan et al., “Communication-efficient learning of deep networks from decentralized data,” in *AISTATS*, 2017.
- [2] P. Kairouz et al., “Advances and open problems in federated learning,” *Found. Trends Mach. Learn.*, 2021.
- [3] M. Abadi et al., “Deep learning with differential privacy,” in *CCS*, 2016.
- [4] K. Bonawitz et al., “Practical secure aggregation for privacy-preserving machine learning,” in *CCS*, 2017.
- [5] L. Atzori et al., “The Internet of Things: A survey,” *Comp. Netw.*, 2010.
- [6] M. Chiang and T. Zhang, “Fog and IoT: An overview of research opportunities,” *IEEE IoT J.*, 2016.
- [7] W. Y. B. Lim et al., “Federated learning in mobile edge networks: A survey,” *IEEE Commun. Surv. Tutor.*, 2020.
- [8] Y. Liu, J. Zhang, and K. Letaief, “Client-edge-cloud hierarchical federated learning,” in *ICC*, 2020.
- [9] C. Shi et al., “Communication-efficient federated learning for IoT,” *IEEE IoT J.*, 2020.
- [10] D. Yin et al., “Byzantine-robust distributed learning,” in *ICML*, 2018.
- [11] P. Blanchard et al., “Machine learning with adversaries: Byzantine tolerance,” in *NeurIPS*, 2017.
- [12] M. Fang et al., “Local model poisoning attacks to federated learning,” in *USENIX Security*, 2020.
- [13] E. Bagdasaryan et al., “How to backdoor federated learning,” in *AISTATS*, 2020.
- [14] A. Reisizadeh et al., “FedPAQ: Communication-efficient federated learning,” in *AISTATS*, 2020.
- [15] D. Alistarh et al., “QSGD: Communication-efficient SGD via quantization,” in *NeurIPS*, 2017.
- [16] H. Lin et al., “DeepFed: Federated deep learning with model/data parallelism,” *IEEE IoT J.*, 2021.
- [17] E. Candès and B. Recht, “Exact matrix completion via convex optimization,” *Found. Comput. Math.*, 2009.
- [18] Y. Aono et al., “Privacy-preserving deep learning via homomorphic encryption,” *IEEE TIFS*, 2018.
- [19] C. Zhang et al., “BatchCrypt: Efficient homomorphic encryption for FL,” in *USENIX ATC*, 2020.
- [20] W. Hu et al., “Open Graph Benchmark,” in *NeurIPS*, 2020.
- [21] M. Ferrag and L. Maglaras, “Edge-IoTSet: Industrial IoT dataset for anomaly detection,” *UCI Repository*, 2020.
- [22] L. Zhu, Z. Liu, and S. Han, “Deep Leakage from Gradients,” in *Advances in Neural Information Processing Systems (NeurIPS)*, 2019, pp. 14774–14784.
- [23] Y. Wu, S. Zhang, X. Zhu, and D. Song, “Model Reconstruction Attacks against Federated Learning: A Projection-based Framework,” in *Proceedings of the 40th International Conference on Machine Learning (ICML)*, 2023.
- [24] J. Geiping, H. Baharav, J. Yan, L. Van der Maaten, M. Goldstein, and T. Goldstein, “Inverting Gradients — How Easy Is It to Break Privacy in Federated Learning?,” in *Proceedings of the International Conference on Learning Representations (ICLR)*, 2021.